



Research article

Synthesis, structural characterization, and DFT studies of anti-cancer drug *N*-(2-Aminophenyl)-2-(4-bromophenoxy)acetamide

S.N. Chandana^a, Fares Hezam Al-Ostoot^{b,c}, Yasser Hussein Eissa Mohammed^{b,d},
Tareq N. Al-Ramadneh^e, P. Akhileshwari^f, Shaukath Ara Khanum^b, M.A. Sridhar^f,
B.N. Lakshminarayana^{a,*}

^a Department of Engineering Physics, Adichunchanagiri Institute of Technology, Jyothinagara, Chikkamagaluru 577102, Karnataka, India

^b Department of Chemistry Yuvaraja's College, University of Mysore, Mysore, Karnataka, India

^c Department of Biochemistry, Faculty of Education and Science, Al-Bayudha University, Yemen

^d Department of Biochemistry, Faculty of Applied Science, University of Hajar, Yemen

^e Department of Basic Science, Biology Unit, Deanship of Preparatory Year and Supporting Studies, Imam Abdul Rahman Binn Faisal University, Saudi Arabia

^f Department of Studies in Physics, Manasa Gangotri, University of Mysore, Mysuru 570006, Karnataka, India

ARTICLE INFO

Keywords:

XRD
Docking analysis
3D-interaction energies
Hirshfeld surface
DFT

ABSTRACT

Drug design is an integrated and developing system that portends an era of a novel and safe tailored drugs. It involves studying the effects of biologically active synthetic, semi-synthetic, and natural compounds based on molecular interactions in terms of molecular structure with activated functional groups or its unique physico-chemical properties involved. The title compound, *N*-(2-aminophenyl)-2-(4-bromophenoxy) acetamide (c), was synthesized in a good yield and characterized by different spectroscopic techniques (¹H, ¹³CNMR, and LC-MS) and finally, the structure was confirmed by X-ray diffraction (XRD) studies. The XRD data confirms that the crystal structure is orthorhombic with space group of *Pca2₁*. The intermolecular interactions (N–H ... O and N–H ... Cg) inside the molecule stabilizes the crystal structure. The existence of this intermolecular interactions are computed by the Hirshfeld surfaces (HS) and two-dimensional (2D) fingerprints plot analysis. In addition to this, Energy frame work analysis is performed to quantify the interaction energies between the molecular pairs in a crystal by incorporating new version of CrystalExplorer17 using the energy model of HF/3-21G. Also to calculate the HOMO and LUMO energies, DFT calculations were carried out.

1. Introduction

In chemotherapy, an effective drug molecule should be capable of interacting with a target protein in the body to reach the target receptor and achieve the goal of the treatment [1, 2]. Systematically, the medicinal chemist has to observe the exact contributions in which each functional group makes to the relative physical and chemical properties of the molecule to determine how these modifications impact biological actions to design better medicinal agents to meet the growing challenges in finding selective drugs [3, 4, 5]. As a result, growing knowledge and understanding of the nature of diseases and drugs has progressively resulted in the intentional design, synthesis, and evaluation of candidate drug molecules. Matrix metalloproteinase (MMP) are recognized biological objectives involved in tumor progression, innate immunity, homeostatic regulation, destroy pro-apoptotic ligand delivery, and

cell-surface receptor release as well as the cleavage [6]. MMPs as inhibitors play significant roles in tumor treatment by promoting the degradation of the extracellular matrix. Therefore, the design and development of effective and specific inhibitor agents that target these enzymes are still highly pursued. Acetamide nucleus and its derivatives are important drugs classes in medicinal chemistry, and many compounds containing benzamide show significant biological activities [7]. Significant attention has also been given to acetamide molecules because of their broad applications as pharmaceutical agents. From both the theoretical and a practical perspective, their great results are highly encouraging to study these compounds in deeply [8]. The natural and synthetic compounds with acetamide nucleus exhibited diverse pharmacological activities such as anti-cancer [9], anti-angiogenic [10], anti-oxidant [11], anti-metastasis [12], anti-inflammatory [13], anti-microbial [14], tranquilizer [15], analgesic, anti-convulsant etc.

* Corresponding author.

E-mail address: bnlphysics@gmail.com (B.N. Lakshminarayana).

<https://doi.org/10.1016/j.heliyon.2021.e06464>

Received 19 September 2020; Received in revised form 23 October 2020; Accepted 5 March 2021

2405-8440/© 2021 The Author(s). Published by Elsevier Ltd. This is an open access article under the CC BY-NC-ND license (<http://creativecommons.org/licenses/by-nc-nd/4.0/>).

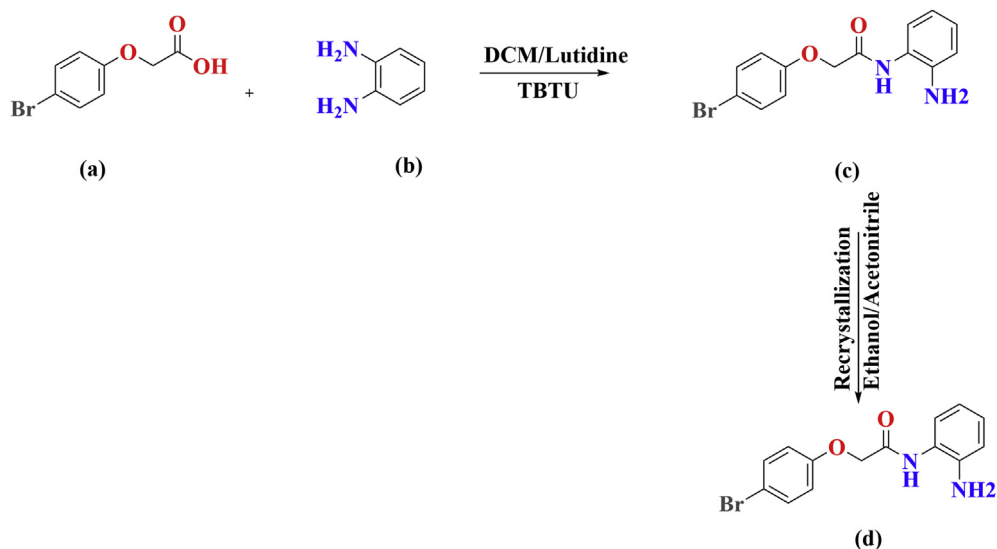


Figure 1. Synthesis of the title compound (c).

[16] and the acetamide residue is found in many proteins [17]. Therefore, the design of new acetamide drugs with less toxicity and a lesser side effect is frequently used in medicinal chemistry, representing a wide range of various biological activities. Because of this application and as part of our on-going work [18, 19, 20], the title compound is synthesized and their structural characterization was studied by single-crystal XRD technique. Molecular docking and Hirshfeld surface investigations also supported the study, which highlighted the interaction of this compound as a very promising MMP-2 inhibitor.

2. Experimental section

2.1. Materials and methods

All chemicals, solvents and starting materials were procured from TCI Chemical Pvt. Ltd., Sigma Aldrich, and it used without further purification. Chemi Line CL 725 Microcontroller based with melting point apparatus with digital thermometer used to determine melting point. The NMR spectrum (^1H and ^{13}C) was documented on a VNMRS-400 MHz Agilent-NMR spectrophotometer in DMSO, and Mass spectra was

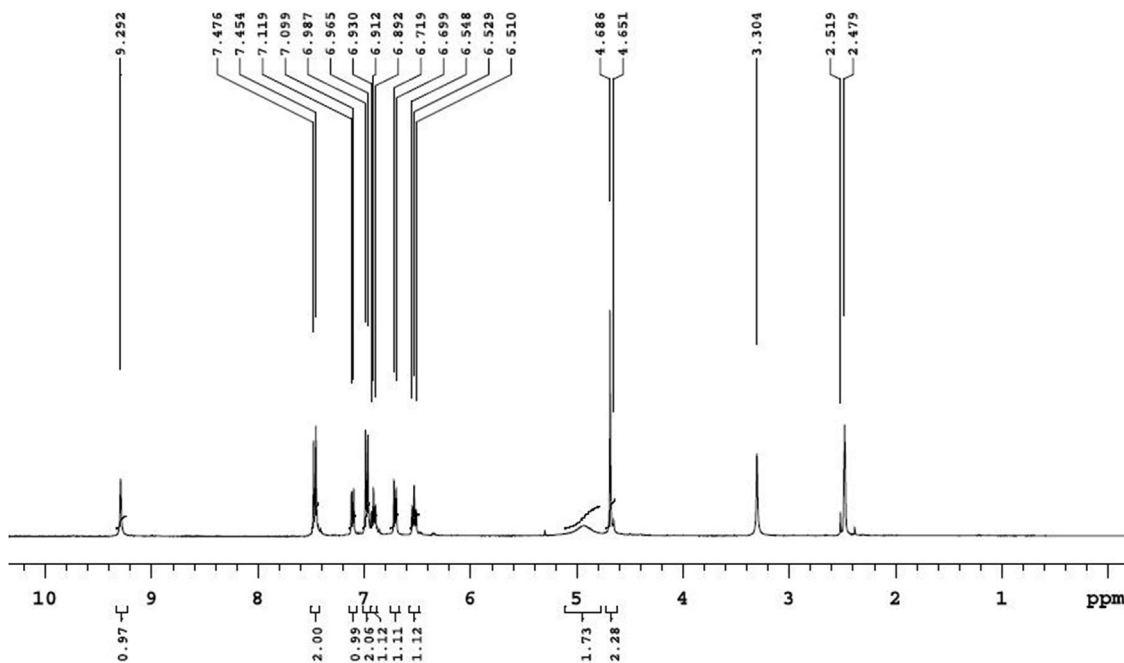


Figure 2. ^1H NMR spectrum of synthesized compound (c).

Table 1. Experimental data and structure refinement details.

Molecular formula	C ₁₄ H ₁₃ Br N ₂ O ₂
Molecular weight	321.17
Density	1.613 Mg m ⁻³
Space group	Pca2 ₁
Crystal system	Orthorhombic
Wavelength and Radiation type	0.71073 Å and MoK _α
θ range for data collection	2.44°–28.32°
Unit cell parameters (Å)	a = 10.426 (3) Å, b = 13.904 (4) Å, c = 9.123 (2) Å
Volume (Å ³)	1322.5 (4)
Z	4
Temperature (K)	296 K
absorption coefficient μ(mm ⁻¹)	3.107
F ₀₀₀	648
Crystal size (mm)	0.22 × 0.21 × 0.20
Diffractometer	Bruker D8 Quest Eco
T _{min} , T _{max}	0.510, 0.537
Reflections collected	11923
Data/restraints/parameters	2871/1/172
Data/restraints/parameters	2871/1/172
Index ranges	h = -13→13, k = -18→17, l = -8→12
Refinement method	least-squares method
Goodness-of-Fit	1.028
R values	R1 = 0.0357, wR2 = 0.0777
Δρ _{max} , Δρ _{min} eÅ ⁻³	0.27, -0.25

obtained with a VG70-70H spectrophotometer. The elemental analysis results are within ±0.4% of the calculated value.

2.2. Synthetic procedure of N-(2-aminophenyl)-2-(4-bromophenoxy)acetamide (c)

The synthesis and synthetic procedure of the title compound (c), as shown in Figure 1. The 4-bromophenoxy acid (a, 0.008 mol) was dissolved in dry Dichloromethane (DCM, 15 mL), and lutidine was added at room temperature, followed by the addition of 1,2-diaminobenzene (b, 0.008 mol), Then the reaction mixture was stirred at the same environment for 30 min. The reaction was cooled in an ice bath to 0–5 °C, 2-(1H-benzotriazole-1-yl)-1,1,3,3-tetramethylammonium tetrafluoroborate (TBTU, 0.02 mol) was added over 30 min while maintaining the

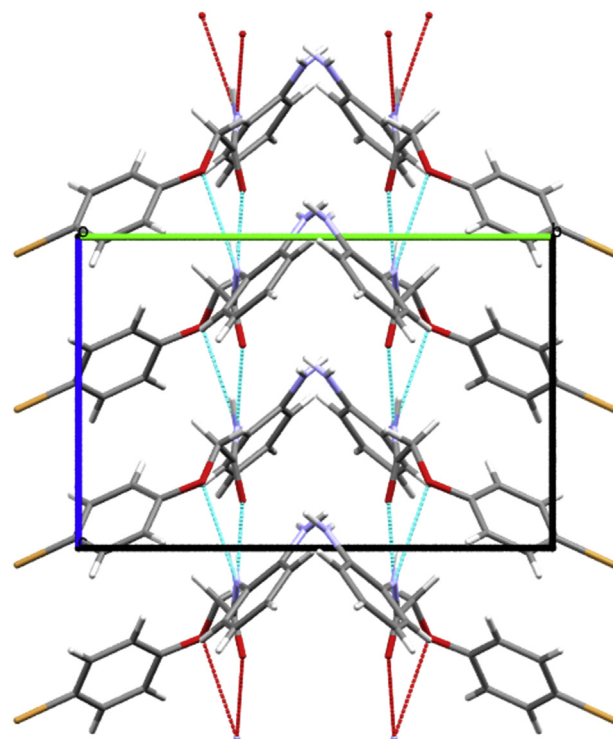


Figure 4. Molecular packing viewed along *a* axis, and intermolecular interactions.

temperature below 5 °C. Later, the reaction was stirred overnight and monitored by TLC using the mobile phase system [hexane: ethyl acetate (6:2)]. The reaction mixture was diluted with 30 mL of DCM and treated with 1.5N hydrochloric acid solution (25 mL). The organic layer was washed with water (3 × 30 mL) and brine (3 × 30 mL). Finally, the organic layer was dried over anhydrous sodium sulfate and concentrated to afford the compound (c) [21, 22]. Then it dried to obtain a crude product which on recrystallization with a mixture of (Ethanol and Acetonitrile) solvents afforded the title compound (c) as a colourless crystal. ¹HNMR spectrum of the synthesized compound (c) was shown in Figure 2.

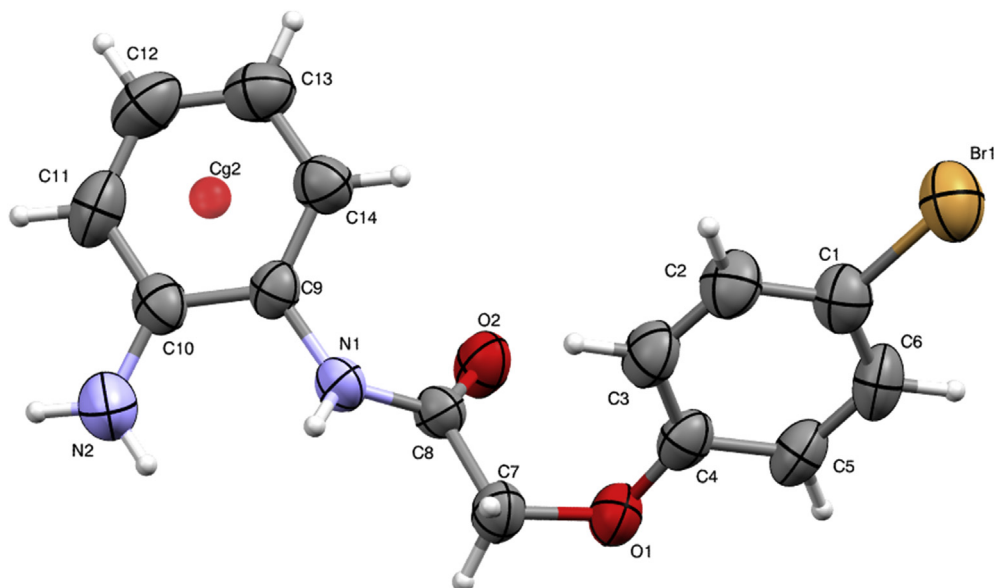
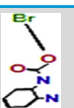
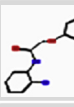
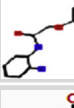
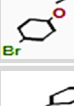
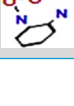
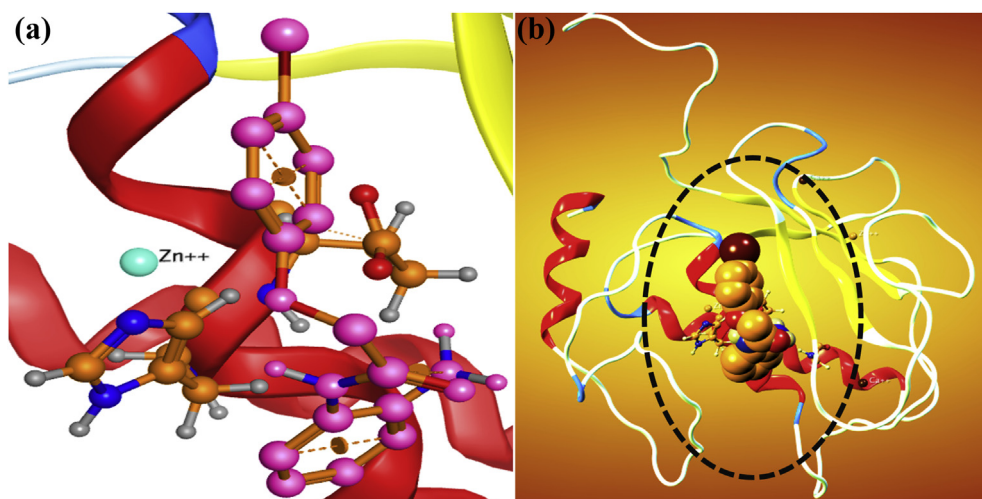


Figure 3. ORTEP diagram of the molecule.

Table 2. Docking energy scores (kcal/mol) derived from the MOE for the complex of MMP-2-c.

Mol	Rseq	Mseq	S	Rmsd-Refine	E_Conf	E_Place	E_Score1	E_Refine	E_Score2
	1	1	-7.4807	3.1178	-10.5306	-60.3399	-9.0050	-58.2949	-7.4807
	1	1	-6.9429	1.3521	-12.6482	-67.7620	-8.6105	-54.5694	-6.9429
	1	1	-6.8631	2.8109	-10.2922	-64.5918	-8.6905	-51.6884	-6.8631
	1	1	-6.5298	1.0206	-8.0021	-39.0260	-9.3818	-30.9748	-6.5298
	1	1	-6.4901	4.4836	-11.8713	-57.5256	-8.7146	-46.5586	-6.4901

**Figure 5.** a) MMP-2 interaction with compound (c) at the pocket site with residue amino acids in MMP-c complex. b) Ribbon diagram of the 1hov and the ligand as a complex molecule.

2.3. Single crystal X-ray diffraction(XRD) analysis

A good quality, suitable, white colored block-shaped single-crystal of the titled compound (c) with the dimensions $0.22 \times 0.21 \times 0.20$ mm was selected for XRD study. The intensity data was recorded on a Bruker D8 quest Eco diffractometer using the radiation of type $M\alpha$ with the wavelength of 0.71073 \AA . SADABS software was used to process the XRD data. The processed XRD data was used to solve the crystal structure by direct methods using the software SHELXT [23] and refined by using SHELXL2018/3 program. All the hydrogen atoms are positioned at chemically accepted positions. PLATON software was used to calculate the geometrical parameters associated with the crystal structure [24]. The ORTEP of the molecule and crystal packing were generated by MERCURY software [25]. The experimental data and refinement details were depicted in Table 1 and the related .cif, .fcf and .checkcif have been included in supplementary files. A list of bond distances (Bond lengths) and angle between three atoms (Bond angles) are tabulated in

Supplementary Table S1 are in agreement with the reported structure [26] and related torsion angles are reported in Supplementary Table S2.

2.4. Molecular modelling studies

2.4.1. Computational method

The crystal structure of MMP-2, a metastasis regulator, was imported from the PDB database with the following [PDB ID: 1hov] [27]. The ligand-receptor complexes were then superimposed over each other. Further the ligand molecule structures were drawn using Chem Draw Professional 16.0, and the energies minimization were performed using Chem3D 16.0. All molecular docking was carried out with the AutoDockTools-1.5.6 (ADT) [28]. This is one of the docking engines with the most common use. Using the ADT, the following multistep process was used for docking ligand to a specific receptor protonation phase, (i) The polar hydrogens were considered, while nonpolar has been merged. (ii) In the next step, Gasteiger charges

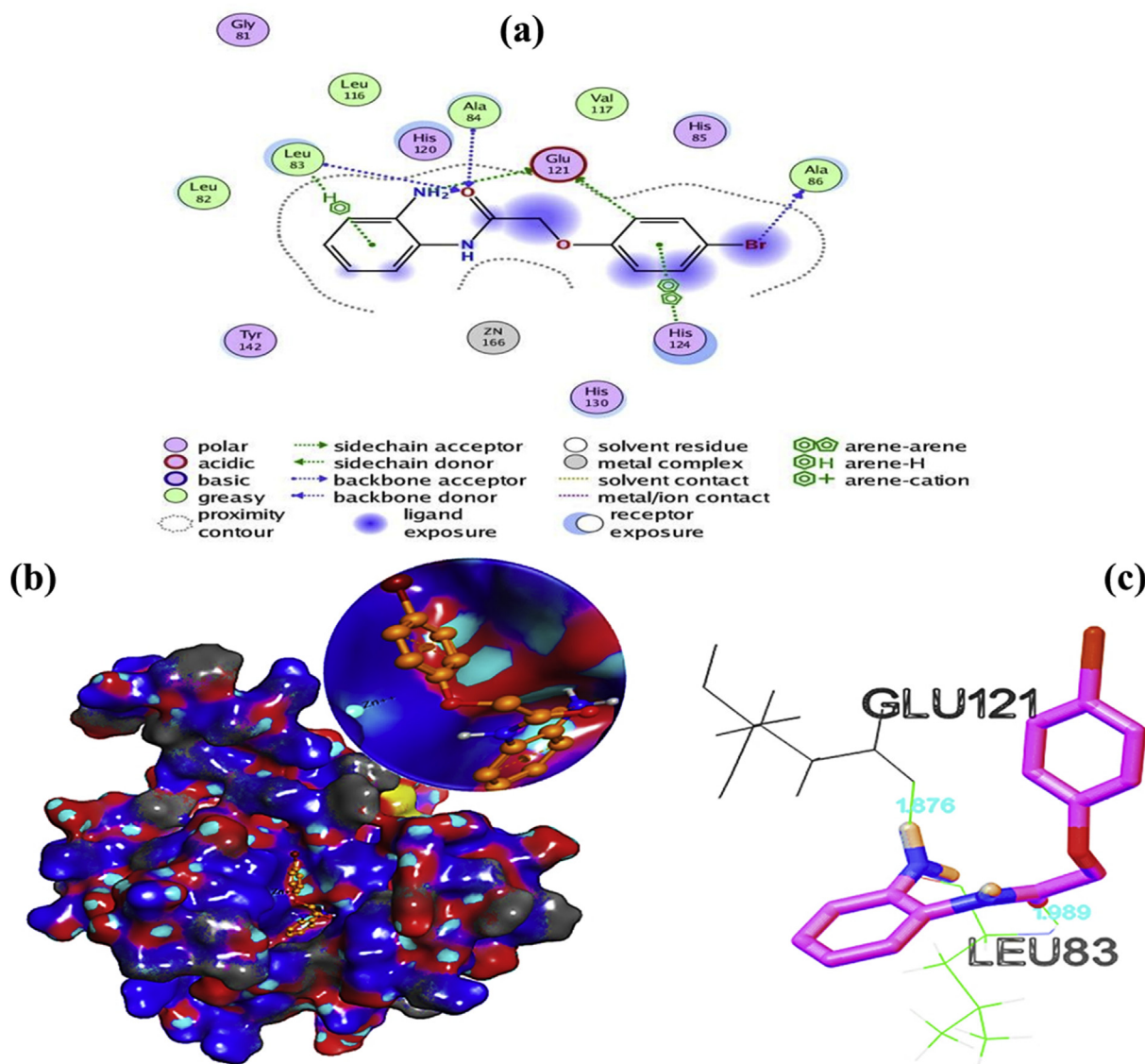


Figure 6. a) The 2D interactions analysis of the title compound with MMP-2. b) 3D representation of the title compound in the active site of MMP-2. c) hydrogen-bond interaction view of the ligand molecule (title compound) with GLU121 and LEU83 in MMP-2 protein.

were also added to the receptors as well as ligands molecules. (iii) A box of size $88 \times 78 \times 102 \text{ \AA}^3$ with a grid spacing of 0.822 \AA was defined around the active site of MMP-2 such that it included all the residues that are critical for the interaction with the inhibitor. (iv) The grid map around each MMP-2 receptor's active site was generated by the probe atoms utilizing the Auto Grid program. Each grid point in the map represents the potential energy of a probe atom in the presence of all the atoms of the receptor molecule. (v) The ligand molecule was docked at the active site MMP-2. The docking calculations were performed by using Lamarckian Genetic Algorithm (LGA) [29]. One hundred runs with 25000000 (maximum) evaluations and 270000 generations were used for the docking simulation. The predictions made by the Auto Dock program were further validated by performing the docking trials using the molecular Operating Environment 2015.10 (MOE) program which was performed on Windows 2010 version to examine the molecular interactions engaged between both the active binding sites of the target protein and the potent

ligand (c) to know the selectivity of the synthesized compounds which can use as anti-cancer drugs [30]. After obtaining docking results and docking and interaction analysis, the resulting best pose score values in the series have been used.

2.5. Hirshfeld surfaces(HS)

The nature and existence of the intermolecular interactions involved in the molecular structure is explored and visualized using HS and its related 2D fingerprint plots. They are obtained by supplying .cif (crystallographic information file) into the Crystal Explorer 17 software [31]. The Hirshfeld surfaces mapped over d_{norm} (normalized contact distance) enables identifying the particular region on the total surface that is involved in intermolecular interactions. The value of d_{norm} may be either negative or positive and is displayed using red, white and blue color scheme used to recognize the shorter and longer intermolecular interaction. Red and blue regions on the surface represents the intermolecular

contacts shorter and longer than the van der Waals radii with negative and positive d_{norm} values respectively whereas the white region denotes the neutral contacts with zero d_{norm} value. Apart from these, the intense red-colored circular spots on the d_{norm} surface always arise due to the presence of D–H ... A type of hydrogen bonding interaction which takes a prime role in the formation of the crystal. The Hirshfeld surface was also mapped on the property of electrostatic potentials using the basis set of Hartee-Fock (HF) [32] level theory to confirm donor and acceptor potentials reveal close contacts in the crystal.

The decomposed form of D–H ... A interaction can be studied using two-dimensional fingerprint plots. It also provides the information on the summary of intercontacts and their percentage of contribution towards crystal packing.

2.6. 3D-energy frameworks

The analysis and calculations of pairwise interaction energies within a crystals plays a vital role in the crystal packing and intermolecular interactions. Owing to the above importance, the authors have studied interaction energies for the compound(c) using the new feature HF/3-21G of CRYSTAL Explore 17 software [33, 34]. It was used to compute interaction energies between the molecular units in a crystal. This can be performed by providing final refined .cif file into the CrystalExplorer17.

3. Results and discussion

3.1. Spectral data

3.1.1. N-(2-aminophenyl)-2-(4-bromophenoxy)acetamide (c)

Yield 70%; m.p.166–169 °C; ^1H NMR (400 MHz, DMSO- d_6) δ (ppm): 4.65 (s, 2H, OCH $_2$), 4.68 (s, 2H, NH $_2$), 6.52–7.41 (m, 8H, Ar–H), 9.14 (s, 1H, NH); ^{13}C NMR (DMSO- d_6) δ : 67.54, 112.97, 116.24, 116.55, 117.47, 122.70, 126.48, 126.87, 132.55, 143.05, 157.62, 166.76; LC–MS m/z : 320 [M+], 322 [M+2]. Anal. Calcd. for C $_{14}$ H $_{13}$ BrN $_2$ O $_2$ (320): C, 60.77; H, 4.74; N, 10.12 Found: C, 60.75; H, 4.72; N, 10.10 %

3.2. Crystal and molecular structure

The titled molecule (c) comprises 2-aminophenyl and 4-bromophenyl rings connected by –NH–C=O–(CH $_2$) = O chain whose displacement ellipsoidal plot (ORTEP) is drawn 50% of probability level is shown in Figure 3. The structure adopts a non-planar structure with a dihedral angle of 52.1 (2)° between terminal phenyl rings (C9/C14) (C1/C6) with maximum deviation (root mean square) of 0.008Å for C8 atom. The torsion angles between the –NH–C=O–(CH $_2$) = O bridge and the aminophenyl (C9/C14) and bromophenyl (C1/C6) rings are 75.4 (5)° (C4–O1–C7–C8), 132.1 (4)° (C8–N1–C9–C10), –5.1 (5)° (C9–N1–C8–O2) also reveals the non-planarity of a molecule. Further, in the molecular structure, bromine and amine (–NH $_2$) substituent's at C1 and C10 on the terminal phenyl rings were adopted + *anti-periplanar* and –*anti-periplanar* confirmation with the torsion angles of Br1–C1–C2–C3 = 179.4 (4)° and N2–C10–C11–C12 = –179.5 (5)° respectively. In a crystal structure, molecules are interconnected by N1–H1 ... O1, N1–H1 ... O2 intermolecular hydrogen bond interactions (shown in Supplementary Table S3). The molecule exhibits one-dimensional independent polymeric chains propagate in the direction of the crystallographic *a*-axis (Figure 4). The molecular structure is also stabilized by the N–H ... π intermolecular interaction of the type N2–H2A ... Cg2, Cg2 is the centroid of the amino phenyle ring (C9–C14) (Figure 3) with an N–Cg distance of 3.477 Å, H...Cg distance of 2.96 Å, N–H...Cg angle of 121°, and with a symmetry code 1–X, 3–Y, –1/2 + Z.

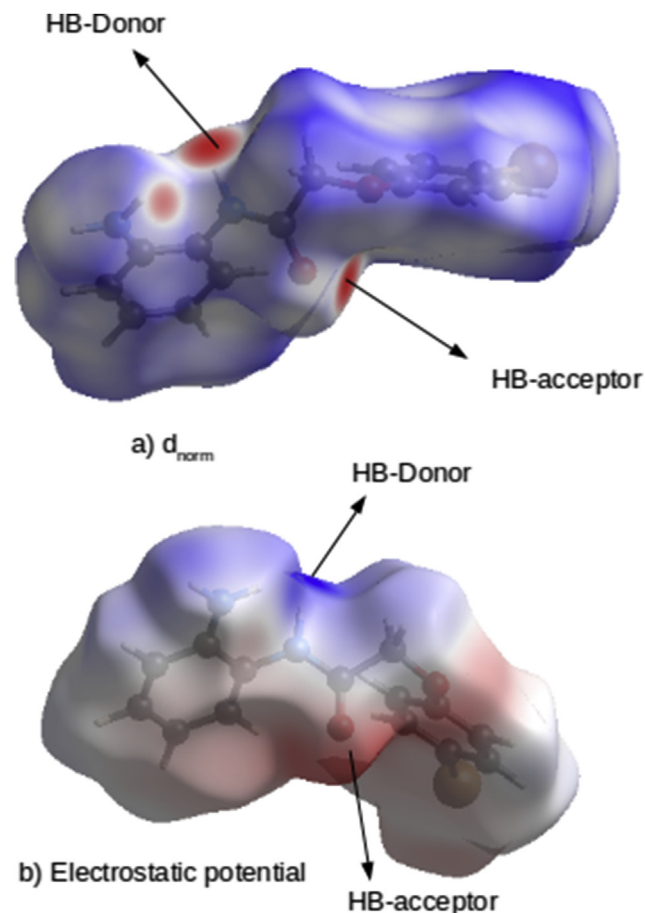


Figure 7. a) The 3D Hirshfeld surface mapped on d_{norm} and b) electrostatic potential.

3.3. Molecular docking analysis and molecular dynamics simulation methods

3.3.1. Ligand (c) interacts with MMP-2

By following the standard procedures [27, 30], the molecular docking was carried out, as well as the analysis showed that the molecule (c) has highly interacted with MMP-2 protein. With particular docking parameters and scoring functions, the ligand's crystal poses were initially re-docked into the exact binding site of target MMP-2 to confirm whether the docking software ADT was suitable for the MMP-2. In addition, the generated (10) conformations were then compared to the various poses of the crystal structure. This implied that ADT was suitable for the MMP-2 and then could properly reproduce the crystal binding model. To achieve the starting model for subsequent molecular docking simulations, the ligand was docked into the same binding pocket site of MMP-2 using the same optimum docking conditions mentioned above. To better understand how ligand influences the binding mode with MMP-2, the structural changes of the two complexes were examined. To visualize, the results are overlapped during the molecular docking simulations of which coordinates were also saved. To know the compound's selectivity for MMP-2, and by helping of AD tools, docking studies were conducted out to examine the molecular interactions occurring between both the target proteins' active binding site and the ligand (c). Based on its lowest binding energy involved in the complex formation at the exact active sites, the inhibitory activity of the MMP-2 was then detected. The docked compound's binding energies on MMP-2 were found in the range of –6.49

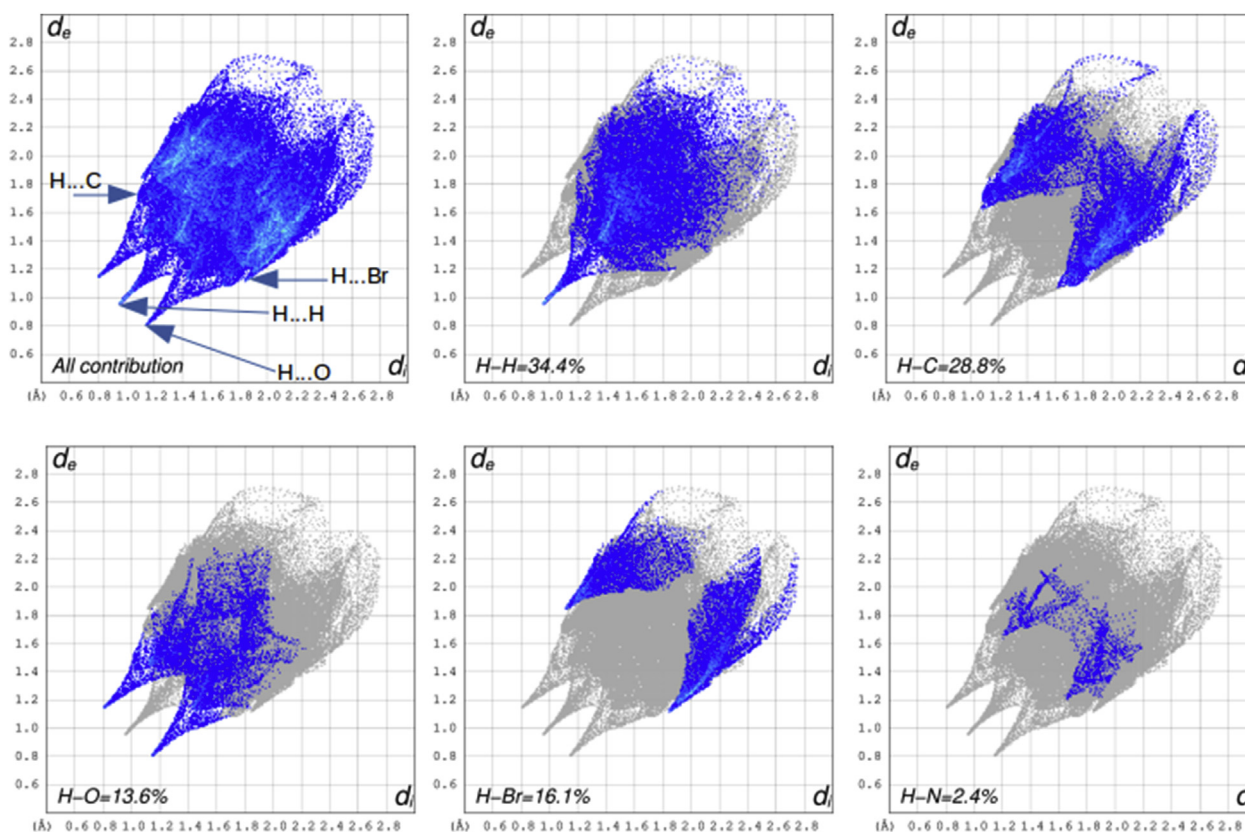


Figure 8. Two-dimensional fingerprint plots of the compound (c).

to -7.48 kcal/mol as shown in Table 2. Several amino acid residues are involved in a particular binding mode; however, different hydrogen bonds interactions could be observed between the ligand (c) and MMP-2 which means that this ligand is stable throughout the molecular docking simulation as shown in Figures 5 and 6. The Ramachandran plot illustrates the MMP-2 modelled protein's phi/psi values. Moreover, the graph presents the rotamer energy plots, residue clashing and contact energy profile of amino acid residues of the MMP-2 proteins' amino acid residues, as shown in Supplementary Figure S1. The docking analysis revealed that the compound (c) could be selected for more investigation in further as a metastasis inhibitor targeting cancer disease.

3.4. Hirshfeld surface calculations

Hirshfeld surface of the compound (c) is mapped with d_{norm} was generated over a fixed color scale of -0.5122 au (red) and 1.3642 au (blue) as shown in Figure 7a. The intense red-colored circular spots marked as 1 and 2 on the d_{norm} is due to the presence of N1-H1 ... O1 and N1-H1 ... O2 contacts, respectively as shown in Supplementary Table S3. Also, the electrostatic potential (Figure 7b) mapped over Hirshfeld surfaces visualizes the intermolecular interaction responsible for molecular packing in the crystal. The red and blue regions on the surface corresponds to negative (hydrogen bond acceptors) and positive (hydrogen bond donors) electrostatic potentials respectively.

The 2D fingerprint plots were obtained in an expanded mode for all available pairs of contacts, as shown in Figure 8. It provides the most useful information, such as a summary of the interaction between various pairs of contacts available towards crystal packing. The final results of two-dimensional fingerprint calculations of a compound (c) depicts that a

pair of H ... H interactions have a significant contribution of 34.4% emerged as a pair of spikes fused almost in the same region of $0.92\text{\AA} < (d_e + d_i) < 0.93\text{\AA}$ followed by another significant contribution of 28.8% from the pair of H ... C contacts which were reflected as unique wings allaying in the region of $1.12\text{\AA} < (d_e + d_i) < 1.66\text{\AA}$. The contribution of H ... Br contacts to HS area is 16.1% seen as two independent symmetric wings over the region of $1.18\text{\AA} < (d_e + d_i) < 1.85\text{\AA}$. The interaction between H and heteroatom (O) which is H ... O pair of contacts contributed about 13.6% appeared in the form of two sharp spikes like pattern spread in the region of $0.8\text{\AA} < (d_e + d_i) < 1.15\text{\AA}$, whereas the H ... N interaction was observed as the least contribution. Only 2.4% can be viewed as blue colored spots spread over the region $1.25\text{\AA} < (d_e + d_i) < 1.65\text{\AA}$.

3.5. Energy framework analysis

The final validated cif is made available as input to the Crystal Explorer program [35] of latest version and the pairwise interaction energies are calculated by constructing a cluster of molecules within a radius of 3.8\AA for a chosen reference molecule and energy frameworks were constructed using CE-HF/3-21G energy model shown in Figure 9.

The total interaction energy is shown in a component form such as E_{ele} , E_{pol} , E_{dis} , and E_{rep} , in Supplementary Figure S2. In each case, the interaction energy was mapped to its constituents of a cluster using cylinders of size 200 (for clear visualization of inter-actions) with 10 kJmol^{-1} of cut-off energy values (to avoid clumsiness due to presence of weak interactions) and scale factors used for benchmarked energies are $k_{\text{ele}} = 1.019$, $k_{\text{pol}} = 0.651$, $k_{\text{disp}} = 0.901$, $k_{\text{rep}} = 0.811$. The cylinders of different thickness represent the relative strength of the interaction between the original one with its constituents in a crystal. It has used red,

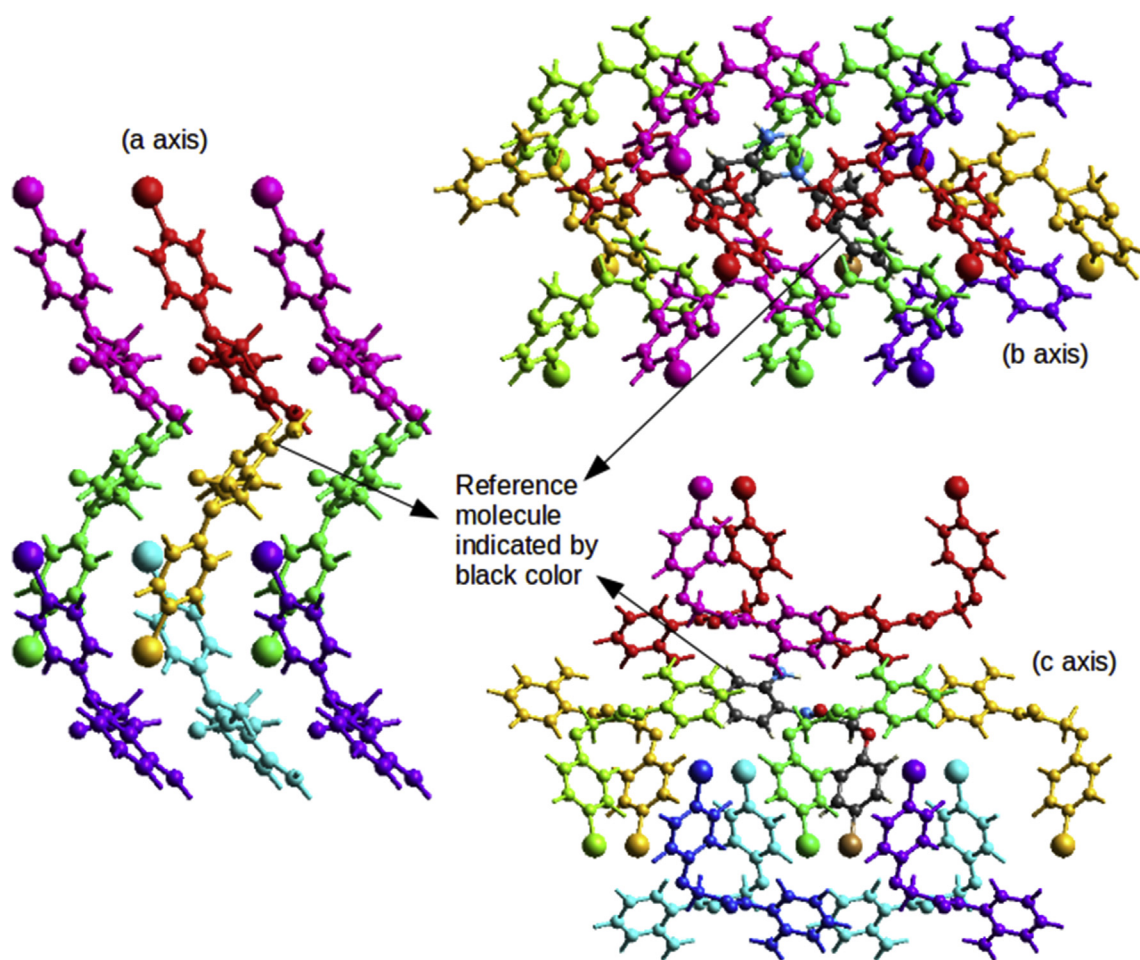


Figure 9. Color code mapping of a cluster's constituents with respect to reference molecule.

green, and blue colors in electrostatic, dispersion, and total energy frameworks. In the three-dimensional energy framework, the maximum interaction energy of -60.9 kJmol^{-1} was noticed for the molecules at 4.62 \AA . Coincidentally the dispersion and total energies were also observed as maximum for the same members of a cluster with -57.1 kJmol^{-1} and -85.4 kJmol^{-1} , respectively. These values are very useful to calculate lattice energies in a molecular crystal. The interaction energy calculations are exhibited in Figure 10. 'R' in the figure indicates the distance between the molecular centroids (mean atomic position) in \AA , Symp represents the symmetry operation. The overall energy framework study reveals that dispersion E_{dis} interaction energies dominated the E_{ele} electrostatic energy.

4. DFT and frontier orbitals of a molecule

Frontier molecular orbitals (FMO) such as Highest occupied molecular orbitals (HOMO) and lowest unoccupied molecular orbitals (LUMO) play a predominant role in the kinetic stability of a molecule in a crystal. Hence Frontier molecular orbitals were analysed through Density functional theory (DFT) by using Gamess software with 6-31G (d,p) basic set at the B3LYP level [36, 37]. The HOMO has the capacity to donate an electron whereas LUMO has the capacity to accept an electron. The energy gap between HOMO and LUMO plays major role in describing the ability of a molecule to transfer the charges. When the orbital energy gap between them is small, the molecule will be more reactive. The

	N	Symp	R	Electron Density	E_ele	E_pol	E_dis	E_rep	E_tot
	2	x+1/2, -y, z	10.52	HF/3-21G	10.3	-6.3	-25.0	15.3	-3.7
	2	x, y, z	10.43	HF/3-21G	1.4	-0.5	-6.4	0.8	-4.0
	2	-x+1/2, y, z+1/2	10.73	HF/3-21G	-1.6	-1.4	-12.6	5.3	-9.7
	2	-x+1/2, y, z+1/2	4.62	HF/3-21G	-60.9	-22.7	-57.1	52.9	-85.4
	2	x+1/2, -y, z	7.06	HF/3-21G	-6.3	-1.4	-22.5	13.1	-17.0
	2	-x, -y, z+1/2	7.98	HF/3-21G	0.5	-0.3	-7.5	2.4	-4.5
	2	-x, -y, z+1/2	8.87	HF/3-21G	-3.6	-1.3	-17.6	8.1	-13.8
	2	-x, -y, z+1/2	11.16	HF/3-21G	-18.4	-7.2	-19.3	9.7	-32.9

Figure 10. Interaction energies (kJ/mole) of Molecular pairs.

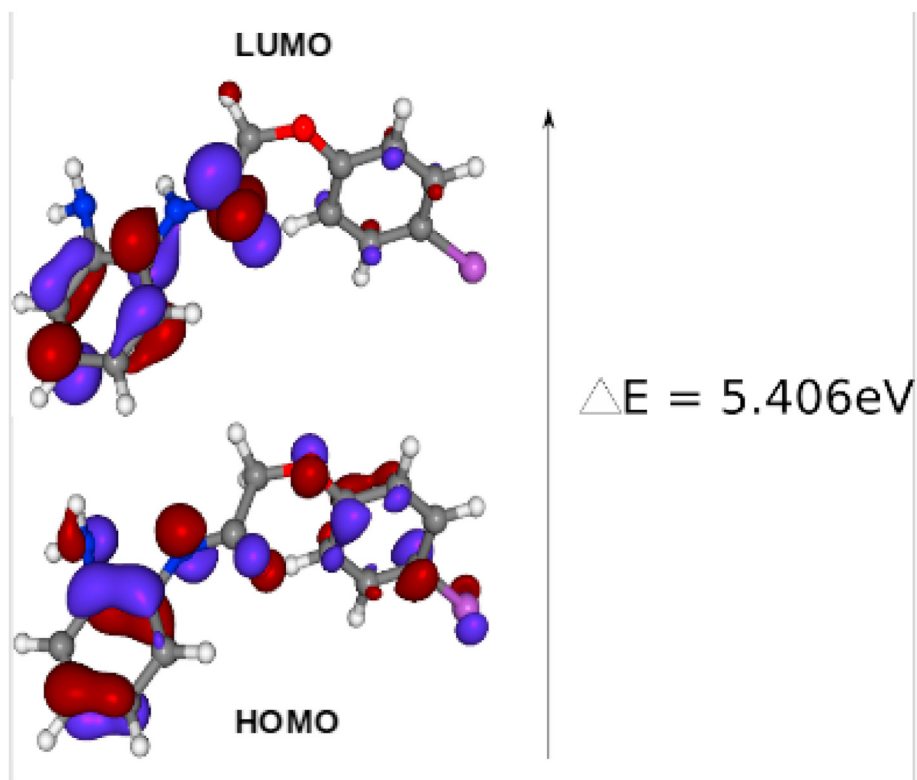


Figure 11. HOMO and LUMO

Table 3. Global descriptive parameters and calculated energy values.

Chemical parameters	Values
E_{HOMO}	-5.8095eV
E_{LUMO}	-0.4027eV
E_{gap} (eV)	5.406eV
Ionization potential(I)	5.8095eV
Electron affinity(A)	0.4027eV
Chemical hardness (η)	2.703eV^{-1}
Global softness (σ)	0.369eV
Chemical potential (μ)	-3.106eV
Electronegativity (χ)	3.106eV
Electrophilicity (ω)	1.784eV

calculated HOMO-LUMO gap of the molecule is 5.406eV, which shows that the molecule is less reactive and highly stable. The molecular orbital pictures of HOMO and LUMO are depicted in Figure 11. This shows HOMO is concentrated over the whole molecule, and LUMO is more concentrated over the amino phenyl ring. The FMO energies, the band gap energy (E_{gap}), and related global descriptive parameters are calculated and tabulated in Table 3.

5. Conclusion

The compound (c) was crystallized into an orthorhombic crystal system with the space group of $Pca2_1$. The Hirshfeld surfaces and 2D fingerprint plots analysis provided the complete insight into crystal packing and intermolecular interactions. The 3D intermolecular interaction energies between the molecular pair was studied, visualized, and analysed. Their result showed that in the crystal, electrostatic energy E_{ele} was dominated over dispersion E_{dis} energy. The *in-silico* analysis reveals that the title ligand (c) showed good binding energy with a hopeful active molecule for cancer treatment. Interaction energy of the ligand (c)

with MMP -2 protein is (-7.48 kJ/mol) and it suggests that to be selective as an anti-cancer agent with further investigations. The orbital energy gap of 5.406 eV between HOMO and LUMO, specifies the hardness and more stability of the compound.

Declarations

Author contribution statement

Chandana S N, Fares Hezam Al-Ostoot: Conceived and designed the experiments; Performed the experiments; Contributed reagents, materials, analysis tools or data; Wrote the paper.

Yasser Hussein Eissa Mohammed: Performed the experiments.

Tareq N. Al-Ramadneh, Shaukath Ara Khanum, Akileshwari P, Sridhar M.A: Analyzed and interpreted the data.

B. N. Lakshminarayana: Conceived and designed the experiments.

Funding statement

Shaukath Ara Khanum was supported by Karnataka State Council for Science and Technology, Indian Institute of Science (VGST/CISEE/282).

Data availability statement

Data associated with this study has been deposited at Cambridge Crystallographic Data Centre under the accession number CCDC 1956950.

Declaration of interests statement

The authors declare no conflict of interest.

Additional information

Supplementary content related to this article has been published online at <https://doi.org/10.1016/j.heliyon.2021.e06464>.

Acknowledgements

Authors thankful to Department of Physics, Periyar university, Selam -636011, Tamilnadu, India, for XRD, Government of Yemen and Al-Baydha University, Yemen and University of Mysore, Mysore, India, University of Hajjah, Yemen.

References

- [1] S. Senapati, A.K. Mahanta, S. Kumar, P. Maiti, Controlled drug delivery vehicles for cancer treatment and their performance, *Signal Transduct. Target. Ther.* 3 (1) (2018 Mar 16) 7.
- [2] J.G. Christensen, H.Y. Zou, M.E. Arango, Q. Li, J.H. Lee, S.R. McDonnell, S. Yamazaki, G.R. Alton, B. Mroczkowski, G. Los, Cytoreductive antitumor activity of PF-2341066, a novel inhibitor of anaplastic lymphoma kinase and c-Met, in experimental models of anaplastic large-cell lymphoma, *Mol. Canc. Therapeut.* 6 (12) (2007 Dec 1) 3314–3322.
- [3] J.J. Knittel, R.M. Zavod, Drug design and relationship of functional groups to pharmacologic activity, *Foye's Princ. Med. Chem.* 6 (2008) 26–53.
- [4] (a) S.A. Patil, Role of medicinal chemist in the modern drug discovery and development, *Org. Chem. Curr. Res.* 2 (2012) 1:e110; (b) J. Venita, Paul Ehrlich, *Arch. Pathol. Lab Med.* 125 (2001) 1–2.
- [5] W. Stevan, The role of the medicinal chemist in the drug discovery process: current status and future prospects, *Drug Discov.* 6 (2005) 9.
- [6] F. Mannello, Natural bio-drugs as matrix metalloproteinase inhibitors: new perspectives on the horizon? *Recent Pat. Anti-Cancer Drug Discov.* 1 (1) (2006 Jan 1) 91–103.
- [7] M.J. Evans, B.F. Cravatt, Mechanism-based profiling of enzyme families, *Chem. Rev.* 106 (8) (2006 Aug 9) 3279–3301.
- [8] G. Sharma, S. Anthal, D.V. Geetha, F.H. Al-Ostoot, Y.H. Hussein Eissa Mohammed, S. Ara Khanum, M.A. Sridhar, R. Kant, Synthesis, structure and molecular docking analysis of an anticancer drug of n-(2-aminophenyl)-2-(2-isopropylphenoxy) acetamide, *Mol. Cryst. Liq. Cryst.* 675 (1) (2018) 85–95.
- [9] Y.H. Mohammed, V.H. Malojirao, P. Ethirusangu, M. Al-Ghorbani, B.T. Prabhakar, S.A. Khanum, The novel 4-phenyl-2-phenoxyacetamide thiazoles modulate the tumour hypoxia leading to the crackdown of neoangiogenesis and evoking the cell death, *Eur. J. Med. Chem.* 1 (143) (2018) 1826–1839.
- [10] J. Lee, J.S. Shim, S.A. Jung, S.T. Lee, H.J. Kwon, N-Hydroxy-2-(naphthalene-2-ylsulfanyl)-acetamide, a novel hydroxamic acid-based inhibitor of aminopeptidase N and its anti-angiogenic activity, *Bioorg. Med. Chem. Lett.* 15 (1) (2005) 181–183.
- [11] A. Caruso, S. Marzocco, B. Nicolaus, C. Palladino, A. Pinto, A. Popolo, M.S. Sinicropi, G. Tommonaro, C. Saturnino, Acetamide derivatives with antioxidant activity and potential anti-inflammatory activity, *Molecules* 15 (3) (2010) 2028–2038.
- [12] H. Jawed, S.U. Shah, S.U. Jamall, S. Simjee, N-(2-hydroxy phenyl) acetamide inhibits inflammation-related cytokines and ROS adjuvant-induced arthritic (aia) rats, *Int. Immunopharm.* 10 (8) (2010 Aug 1) 900–905.
- [13] G.G. Berest, O.Y. Voskoboinik, S.I. Kovalenko, O.M. Antypenko, I.S. Nosulenko, A.M. Katsev, O.S. Shandrovskaia, Synthesis and biological activity of novel N-cycloalkyl-(cycloalkylaryl)-2-[(3-R-2-oxo-2H-[1, 2, 4] triazino [2, 3-c] quinazoline-6-yl) thio] acetamides, *Eur. J. Med. Chem.* 46 (12) (2011 Dec 1) 6066–6074.
- [14] H.P. Jayadevappa, G. Nagendrappa, S. Umesh, S. Chandrashekar, Synthesis of novel 2-(4-(2-morpholinoethoxy) phenyl)-N-phenylacetamide analogues and their antimicrobial study, *J. Chem. Sci.* 124 (5) (2012 Sep 1) 1019–1023.
- [15] Z.A. Kaplancikli, M.D. Altintop, G. Turan-Zitouni, A. Ozdemir, O.D. Can, Synthesis and analgesic activity of some acetamide derivatives, *J. Enzym. Inhib. Med. Chem.* 27 (2) (2012 Apr 1) 275–280.
- [16] A. Rajasekaran, S. Murugesan, Synthesis and characterization of some novel azetidinone derivatives as anti-bacterial and anti-convulsant agents, *J. Pharm. Bioresour.* 2 (2) (2005) 162–168.
- [17] Y. Özkay, İ. Işıkdag, Z. İncesu, G. Akalin, Synthesis of 2-substituted-N-[4-(1-methyl-4, 5-diphenyl-1H-imidazole-2-yl) phenyl] acetamide derivatives and evaluation of their anticancer activity, *Eur. J. Med. Chem.* 45 (8) (2010 Aug 1) 3320–3328.
- [18] S.M. Kumar, A.O. Hezam, B.C. Manjunath, V.R. Shamprasad, Y.H. Mohammed, N. Mahesh, A.K. Shaikath, N.K. Lokanath, K. Byrappa, Crystal packing analysis of 1-(3, 4-dimethoxyphenyl)-3-(4-bromophenyl) prop-2-en-1-one exhibiting a putative halogen bond CBr...O, *J. Mol. Struct.* 1156 (2018 Mar 15) 216–223.
- [19] K. Kumara, F.H. Al-Ostoot, Y.H. Mohammed, S.A. Khanum, N.K. Lokanath, Synthesis, crystal structure and 3D energy frameworks of ethyl 2-[5-nitro-2-oxo-pyridine-1 (2H)-yl] acetate: Hirshfeld surface analysis and DFT calculations, *Chem. Data Collect.* 20 (2019 Apr 1) 100195.
- [20] S.M. Kumar, B.C. Manjunath, F.H. Al-Ostoot, M. Jyothi, M. Al-Ghorbani, S.A. Khanum, A.K. Kudva, N.K. Lokanath, K. Byrappa, Synthesis, crystal structure and Hirshfeld surfaces of 1-(3, 4-dimethoxyphenyl)-3-(3-hydroxyphenyl) prop-2-en-1-one, *Chem. Data Collect.* 15 (2018 Aug 1) 153–160.
- [21] D.V. Geetha, F.H. Al-Ostoot, Y.H. Mohammed, M.A. Sridhar, S.A. Khanum, N.K. Lokanath, Synthesis, Elucidation, Hirshfeld surface analysis, and DFT calculations of 4-chloro-N-[2-(2-1H-indol-3-yl-acetylamino)-phenyl]-benzamide, *J. Mol. Struct.* 1178 (2019 Feb 15) 384–393.
- [22] F.H. Al-Ostoot, Y.H. Mohammed, A.N. Zabiulla, S.A. Khanum, Synthesis, in silico study and in vitro anti-microbial evaluation of some new N-benzoyl-N'-[2-(4-chlorophenoxy)-acetyl]-hydrazides analogs, *J. Appl. Pharmaceut. Sci.* 9 (7) (2019 Jul) 42–49.
- [23] G.M. Sheldrick, Crystal structure refinement with SHELXL, *Acta Crystallogr. C* 71 (2015) 3–8.
- [24] A.L. Spek, Structure validation in chemical crystallography, *Acta Crystallogr. D* 65 (2) (2009) 148–155.
- [25] Clar F. Macrae, Ian J. Bruno, James A. Chishlom, Paul R. Edgington, Patrick Mc Cabe, Elna Pidcock, Lucia Rodriguez-Monge, Robin Taylor, Jacco Van de Streek, Peter A. Wood, Mercury CSD 2.0-new features for the visualization and investigation of crystal structure, *J. Appl. Crystallogr.* 41 (2) (2008) 466–470.
- [26] N.R. Sreenatha, B.N. Lakshminarayana, D.P. Ganesh, S. Vijaykumar, S. Nagaraju, X ray stucture analysis online 34 (2018) 23–24.
- [27] Y.H. Mohammed, P. Thirusangu, V. Vigneshwaran, B.T. Prabhakar, S.A. Khanum, The anti-invasive role of novel synthesized pyridazine hydrazide appended phenoxy acetic acid against neoplastic development targeting matrix metallo proteases, *Biomed. Pharmacother.* 95 (2017) 375–386.
- [28] Al-Ostoot, Fares Hezam, D.V. Geetha, Yasser Hussein Eissa Mohammed, P. Akhileshwari, M.A. Sridhar, Shaikath Ara Khanum, Design-based synthesis, molecular docking analysis of an anti-inflammatory drug, and geometrical optimization and interaction energy studies of an indole acetamide derivative, *J. Mol. Struct.* 1202 (2020) 127244.
- [29] Yi Fu, Ji Zhao, Zhiguo Chen, Insights into the molecular mechanisms of protein-ligand interactions by molecular docking and molecular dynamics simulation: a case of oligopeptide binding protein, *Comput. Math. Methods Med.* (2018) 2018.
- [30] Y.H. Mohammed, S.A. Khanum, The critical role of novel benzophenone analogs on tumor growth inhibition targeting angiogenesis and apoptosis, *Med. Chem. Comm.* 9 (4) (2018) 639–656.
- [31] M.A. Spackman, D. Jayatilaka, Hirshfeld surface analysis, *Cryst. Eng. Comm.* 11 (2009) 19–32.
- [32] Mark A. Spackman, Joshua J. McKinnon, Dylan Jayatilaka, Electrostatic potentials mapped on Hirshfeld surfaces provide direct insight in to intermolecular interaction in crystals, *Cryst. Eng. Commun.* 10 (4) (2008) 377–388.
- [33] M.A. Spackman, J.J. McKinnon, Finger printing intermolecular interactions in molecular crystals, *Crystal Eng. Commun.* 4 (66) (2002) 378–392.
- [34] Campbell F. Mackenzie, Peter R. Spackman, Dylan Jayatilaka, Mark A. Spackman, Crystal Explorer model energies and energy frameworks: extension to metal coordination compounds, organic salts, solvates and open-shell systems, *IUCr J.* 4 (2017) 575–587.
- [35] M.J. Turner, S. Grabowsky, D. Jayatilaka, M.A. Spackman, Accurate and efficient model energies for exploring intermolecular interactions in molecular crystals, *J. Phys. Chem. Lett.* 24 (2014) 4249–4255.
- [36] M.W. Schmidt, K.K. Baldrige, J.A. Boatz, S.T. Elbert, M.S. Gordon, J.H. Jensen, S. Koseki, N. Matsunaga, K.A. Nguyen, S.J. Su, T.L. Windus, M. Dupuis, J.A. Montgomery, General atomic and molecular electronic structure system, *J. Comput. Chem.* 14 (1993) 1347–1363.
- [37] A.D. Becke, Density-functional thermochemistry. III. The role of exact exchange, *J. Chem. Phys.* 98 (1993) 5648–5652.